ADVANCED FUNCTIONAL MATERIALS
www.afm-journal.de

Materials Views
www.MaterialsViews.com

Synthesis of Optical-Quality Single-Crystal β-BaB_2O_4 Microwires and Nanowires

*Guangyuan Qu, Zhifang Hu, Yipei Wang, Qing Yang, and Limin Tong**

The synthesis of optical quality β-barium borate microwires and nanowires (MNWs) is reported using an organic-free hydrothermal method with $BaCl_2{\cdot}6H_2O$, NaOH, and H_3BO_3 as source materials, and assisted with post-annealing. As-synthesized MNWs, with diameters ranging from 500 nm to 2 μm and lengths up to several hundred micrometers, show good optical-waveguiding capabilities. Based on evanescent coupling between a single BBO MNW waveguide and a fiber taper, propagation losses of 0.30 dB μm^{-1} (at 532 nm) and 0.21 dB μm^{-1} (at 671 nm) are evaluated, respectively. An evident second-harmonic generation (SHG) signal at 532 nm with a measured conversion efficiency of about 8.4% is observed when excited by waveguided 1064 nm, picosecond laser pulses within a BBO MNW with a length of the order of 100 μm. The dependence of the SHG conversion efficiency on the MNW diameter is also investigated. These results show a much-higher SHG efficiency for BBO single-crystal MNWs compared with bulk crystal, which suggests potential applications in future micro-/nanoscale nonlinear optical applications such as optical modulation and frequency conversion.

1. Introduction

In recent years, one-dimensional (1D) micro-/nanostructures, such as microwires and nanowires (MNWs) and microfibers, have attracted considerable attention in optics and photonics applications due to their low dimensionality, tight optical confinement, and excellent waveguiding capabilities. As 1D building blocks for micro-/nanoscale photonic circuits and devices, MNWs with high optical quality and high nonlinearity are of particular importance, and have applications in areas ranging from optical modulation, to wavelength conversion, and near-field imaging.[1–10] One of the most straightforward approaches to fabricating these 1D structures is to synthesize MNWs directly from materials with high nonlinearity, such as semiconductors and inorganic nonlinear optical crystals. Semiconductors (e.g., CdS) typically present high optical nonlinearity, but usually suffer from the disadvantages of significant free-carrier-induced effects, such as two-photon absorption, which results in a high loss and a response time limited by the carrier lifetime and prevents them from being used in ultrafast devices such as optical modulators.[11–15] In contrast, as the most widely used nonlinear optical materials, inorganic nonlinear optical crystals (e.g., β-BaB_2O_4, $LiNbO_3$, LiB_3O_5, KH_2PO_4 and $KTiOPO_4$) exhibit high nonlinearity and also benefit from negligible two-photon absorption and free-carrier effects, a higher quality of the crystal, and a higher damage threshold. With high nonlinearities, excellent chemical and mechanical stability, and the absence of free-carrier effects, inorganic nonlinear optical crystals have been serving as critical materials for fast response and high-bandwidth photonic devices in modern telecommunications. In low-dimensional micro-/nanostructures of these nonlinear crystalline materials, optical nonlinearity is expected to be significantly enhanced due to the tight optical confinement. So far, only a few types of nonlinear crystal MNWs have been synthesized. Recently, individual single-crystalline $LiNbO_3$, $KNbO_3$, and $NaNbO_3$ NWs and nanorods have been synthesized through a hydrothermal reaction and have a broadband waveguiding capability and an efficient second harmonic generation, suggesting the potential of nonlinear optical nano-waveguides for efficient frequency conversion and other purposes.[4,16–18]

As one of the most important nonlinear optical crystals, β-barium borate (β-BaB_2O_4, BBO) crystals have been widely used in second-, third-, fourth-, and fifth-harmonic generation, as well as in optical parametric oscillators (OPO) and optical parametric amplifiers (OPA),[19–22] owing to their high nonlinear optical coefficients, low group-velocity dispersion, broad spectral window of transparency, and high damage threshold.[19,23–26]

Recently, several methods to synthesize 1D BBO nanostructures including nanorods, nanospindles and network-like nanostructure were reported,[27–29] but their uses as nonlinear optical waveguides are limited by the morphology, such as he shape, size, composition, and spatial configuration. Compared with bulk crystals, 1D MNWs can offer tight optical confinement for enhanced field intensity and excellent waveguiding capabilities for greatly enhanced light-material interaction. Here, we report an organic-free hydrothermal method to synthesize BBO MNWs for optical waveguiding with diameters from 500 nm to 2 μm and lengths up to several hundred micrometers. Excited by waveguided 1064 nm, picosecond laser

G. Qu, Z. Hu, Y. Wang, Prof. Q. Yang, Prof. L. Tong
State Key Laboratory of Modern Optical Instrumentation
Department of Optical Engineering
Zhejiang University
Hangzhou, 310027, China
E-mail: phytong@zju.edu.cn

DOI: 10.1002/adfm.201201866

pulses, evident second-harmonic generation (SHG) at 532 nm is observed, with a measured conversion efficiency of about 8.4% within a length of 114 μm, suggesting the possibility of using these BBO MNWs as nonlinear building blocks for future nonlinear micro-/nanophotonic devices.

2. Sample Preparation

In this work, BBO MNWs were synthesized by an organic-free hydrothermal method[30–35] assisted with post-annealing. $BaCl_2 \cdot 6H_2O$, NaOH, and H_3BO_3 with a molar ratio of 1:2:2 were used as starting materials. As illustrated in **Figure 1**a, $BaCl_2$ and NaOH solution were mixed and stirred thoroughly, forming a $Ba(OH)_2$ emulsion, as in reaction 1. H_3BO_3 solution was then added into the generated emulsion, as in reaction 2. After continuous stirring for about 30 min, a homogeneous white slurry was obtained. The slurry was then transferred into an autoclave and heated at temperature of 150–200 °C in an oven for 5 days, resulting in a white, flocculent precipitate deposit at the bottom of the autoclave. After being filtered and washed with deionized water and alcohol for several times, BBO MNWs were obtained in a white precipitate, with the typical morphology shown in Figure 1b. The MNWs obtained at this stage were usually 50 nm to 2 μm in diameter and several hundred micrometers in length, with excellent diameter uniformity and surface quality.

$$BaCl_2 + 2NaOH \rightarrow Ba(OH)_2 + 2NaCl \quad (1)$$

$$Ba(OH)_2 + 2H_3BO_3 \rightarrow BaB_2O_4 + 4H_2O \quad (2)$$

X-ray powder diffraction was used to examine the crystal structure and phase composition of the as-grown MNWs, with the results shown in Figure 1c. The XRD pattern coincides well with JCPDS file no. 35-0181, from which we identify the MNWs to be in the γ-BaB_2O_4 structure, a low-temperature form of BaB_2O_4.[36] Typically, BaB_2O_4 has three forms, γ-BaB_2O_4, β-BaB_2O_4, and α-BaB_2O_4. The γ-BaB_2O_4 form can be transformed to the β-BaB_2O_4 form, and the β-BaB_2O_4 form to the α-BaB_2O_4 form by annealing.[23,24,36] Here, accordingly, to transform the γ-BaB_2O_4 MNWs to β-BaB_2O_4 MNWs, we annealed the γ-BaB_2O_4 MNWs at 700 °C for 1 h in an O_2 atmosphere. The XRD pattern of the as-annealed MNWs is shown in Figure 1d, which is in excellent agreement with the hexagonal phase of β-BaB_2O_4 (JCPDS file no. 80-1489), with lattice constants of $a = b =$ 12.53 Å and c = 12.72 Å, a hexagonal crystal system and space group of R3c (161), without characteristic peaks of any other impurity groups, indicating that the obtained MNWs were in β-BaB_2O_4 form. After the annealing process, the diameter and length of the MNWs were well retained. Figure 1e shows an SEM image of a typical β-BaB_2O_4 MNW 550 nm in diameter and 210 μm in length, corresponding to a length-to-width aspect ratio of about 380.

The morphology of the as-synthesized MNWs was further examined using field-emission scanning electron microscopy (FE-SEM) with a high magnification, as shown in **Figure 2**a,b. Figure 2a gives a close-up image of a 600 nm-diameter γ-BBO MNW, showing excellent diameter uniformity and surface smoothness. Figure 2b gives a close-up image of a 670 nm diameter β-BBO MNW, with the triangular cross-section shown in the inset. It shows that, after annealing, the BBO MNW retains diameter uniformity, while exhibiting relatively higher surface roughness, although there's no significant structural irregularity. Lattice-resolved high-resolution transmission electron microscopy (HR-TEM) images (Figure 2c,d) reveal the microstructures and morphologies of the MNWs. The top insets show the corresponding selected area electron diffraction (SAED) patterns, confirming the single-crystalline β-BaB_2O_4 in the [100] direction in Figure 2d. The lattice-fringe separations were measured to be about 0.37 nm (c) and 0.72 nm (d), respectively. The clear lattice fringe and its corresponding SAED pattern confirm that the BBO MNW was single crystalline, without twin structures, stacking faults, and dislocations.

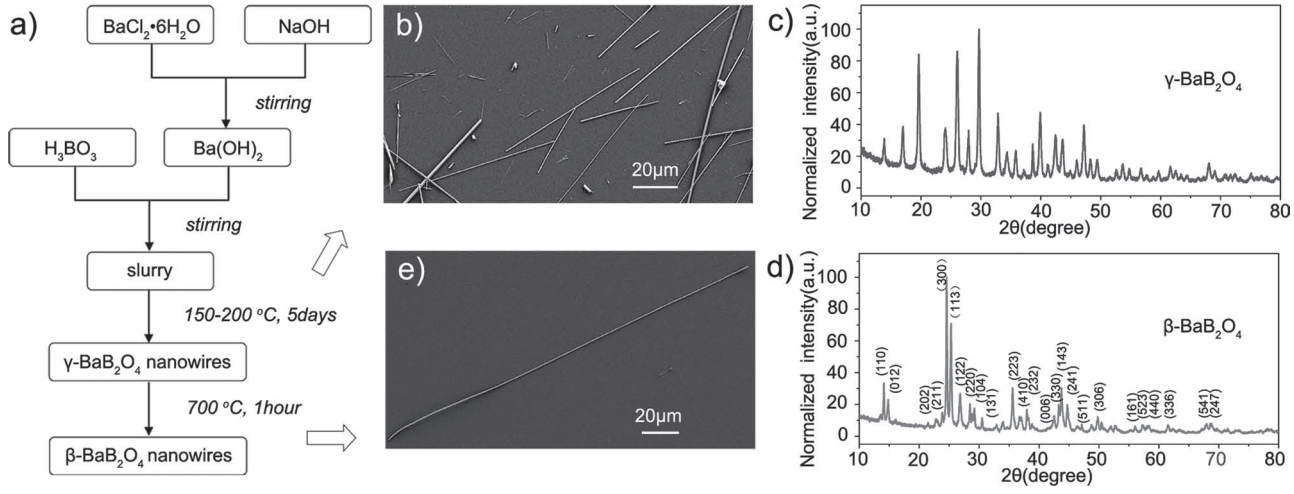

Figure 1. a) Synthesis process for β-BaB_2O_4 MNWs. b) SEM image of γ-BaB_2O_4 MNWs. c,d) XRD patterns of γ-BaB_2O_4 (c) and β-BaB_2O_4 (d) MNWs. e) SEM image of a typical 555 nm-diameter, 210 μm-long β-BaB_2O_4 MNW.

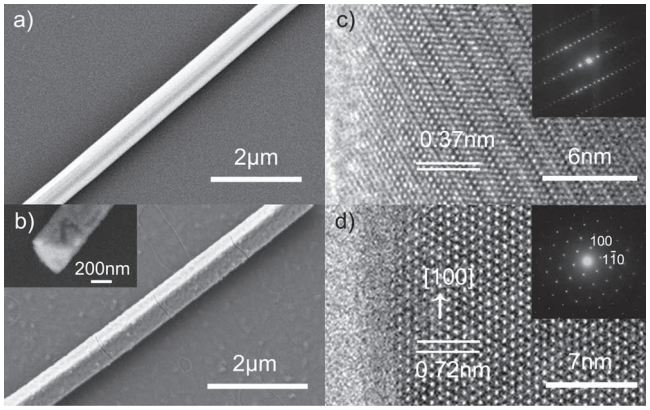

Figure 2. a) Close-up SEM image of a single γ-BaB_2O_4 MNW, with diameter of 600 nm. b) Close-up SEM image of a single β-BaB_2O_4 MNW after annealing, with diameter of 670 nm; the inset shows a close-up image of one end of a 400 nm-diameter β-BaB_2O_4 MNW with a perfect triangular end face. c,d) Lattice-resolved HR-TEM image of a single γ-BaB_2O_4 MNW (c) and a β-BaB_2O_4 MNW (d), with the corresponding SAED patterns (insets).

3. Optical-Waveguiding Properties

Optical characterization of the BBO MNWs was carried out under an optical microscope, as schematically illustrated in **Figure 3**a. As-synthesized BBO MNWs were dispersed on the polished surface of a MgF_2 wafer, which had a refractive index of 1.38 (at wavelength of 550 nm). To launch light efficiently into a single BBO MNW, we used an evanescent coupling technique assisted with a nanoscale fiber taper, which was taper-drawn from a standard optical fiber (Corning SMF-28)[37,38] and mounted on a 3D moving stage for precise coupling with the MNW. The fiber taper maintained a tapering tendency at its distal end, making it possible to match the index of the fiber taper to that of the MNW within the coupling region. The optical-signal output from the MNW was first collected by the same objective lens used for imaging, then directed through a 1064 nm notch filter, and split by a dichroic mirror to a spectrometer and a charge-coupled-device (CCD) camera for spectral measurement and imaging, respectively. All of the measurements were performed at room temperature.

Figure 3b,c shows optical microscopy images of light coupling from a fiber taper to a 2 μm-diameter 100 μm-length BBO MNW, in which the wavelengths of the light were 671 nm and 532 nm, respectively. The images show that light was coupled into the BBO MNW and guided along the axial direction, demonstrating the optical-waveguiding capability of the MNW. Obvious scattering along the entire length of the MNW was induced by the surface roughness (see also Figure 2b), indicating that the waveguiding quality could be further improved.

To evaluate the propagation loss of the BBO MNW, we employed a propagation-distance-dependent output measurement that has been reported elsewhere.[39,40] We moved the fiber taper along the length of the MNW without changing the coupling condition, and recorded the output intensity from the other end of the BBO MNW using a calibrated CCD camera (see Experimental Section).

Figure 3d shows propagation-distance-dependent output intensities of a 580 nm-diameter β-BBO MNW at wavelengths of 532 and 671 nm, respectively (see Supporting Information). The solid curves were fitted to the experimental results using a non-linear least-squares fitting method. Generally, the output intensity $I(x)$ of the MNW exponentially decreases along the axial length according to:

$$I(x) = I_0 \times e^{-x/L_0} \tag{3}$$

where I_0 is the initial intensity, x is the transmission distance along the axial direction, and L_0 is the propagation length.

The propagation length of the BBO MNW (L_0) can be estimated, and is related to the propagation loss by:

$$\alpha = \frac{-10\log(1/e)}{L_0} \approx \frac{4.343}{L_0} \tag{4}$$

Using the fitted curves showed in Figure 3d and Equation 3, we obtained propagation lengths L_0 of 14.4 μm (at 532 nm) and 20.9 μm (at 671 nm) for the 580 nm-diameter BBO MNW, corresponding to propagation losses of 0.30 dB μm^{-1} (at 532 nm) and 0.21 dB μm^{-1} (at 671 nm).

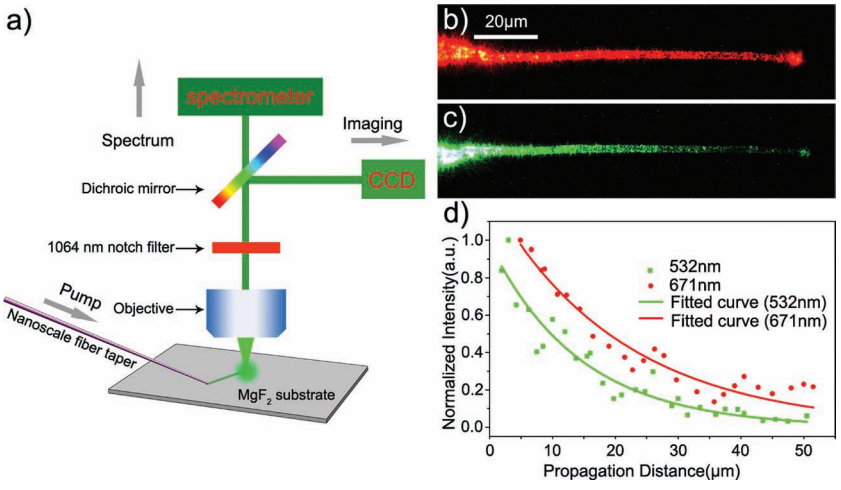

Figure 3. a) Schematic diagram of the experimental setup for optical characterization of the BBO MNWs. b,c) Microscopy images of the transmission of a BBO MNW at wavelengths of 671 nm (b) and 532 nm (c). The same BBO MNW, with a diameter of 2 μm, was used in (b) and (c). d) The propagation-distance-dependent normalized output intensities of a 580 nm-diameter BBO MNW at 532 nm and 671 nm wavelengths respectively. The solid curves show the fitting results of the experimental results.

4. SHG in Single BBO MNWs

To investigate the optical nonlinear properties of a single BBO MNW, we launched 10 ps-duration pulses from a 1064 nm-wavelength YVO_4 laser into one end of an MNW by evanescent coupling, and measured the SHG output of the MNW.

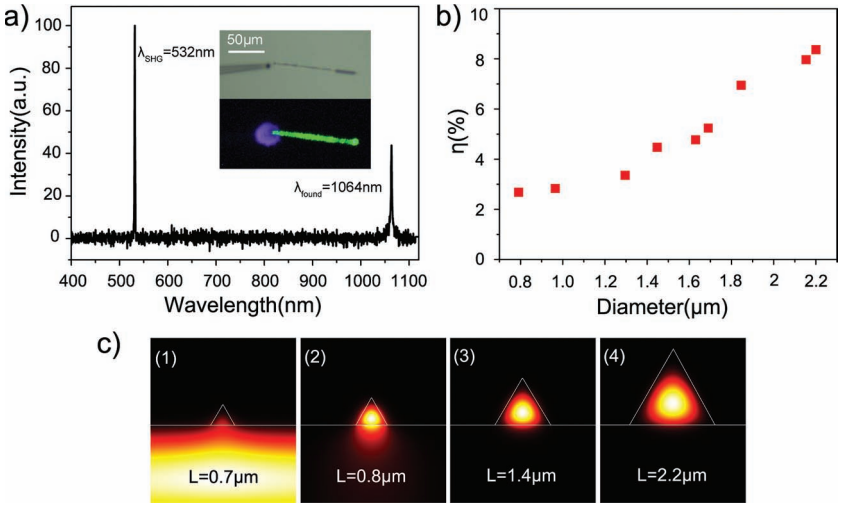

Figure 4. a) SHG spectrum of a single 2.2 μm-diameter BBO MNW excited by 1064 nm-wavelength picosecond pulses, taken with a notch filter with 2% transmission at 1064 nm wavelength, and the corresponding microscope images (inset). b) SHG conversion efficiency of 9 BBO MNWs with different diameters. c) Calculated Poynting vectors for triangular BBO waveguides with side lengths L of 0.7 μm (1), 0.8 μm (2), 1.4 μm (3), and 2.2 μm (4), respectively. The supporting substrate is assumed to be MgF_2.

Figure 4a shows the SHG spectrum of a single, 2.2 μm-diameter, 114 μm-length BBO MNW, excited by 1064 nm-wavelength laser pulses, with experimental details shown in the inset. The SHG spectrum and the optical microscopy images were taken after a notch filter with 2% transmission at a wavelength of 1064 nm. To estimate the efficiency of the SHG, we compared the relative intensity of the pump and the SHG light at the output end of the BBO MNW. The intensity ratio of the 1064 nm pump to the 532 nm SHG signal was 43.8:100. After calibrating the transmission of the notch filter, the estimated conversion efficiency from 1064 nm light to 532 nm light is about 8.4%.

The SHG intensity, $I(2\omega)$, generated from the BBO by a fundamental beam with intensity $I(\omega)$ is given by:[26,41,42]

$$I(2\omega) \propto \left[\frac{l_s^2 I^2(\omega) d_{eff}^2}{n^2(\omega)\, n(2\omega)}\right] \frac{\sin^2\left(\frac{\pi l_s}{2l_c}\right)}{\left(\frac{\pi l_s}{2l_c}\right)^2}$$

$$= \left[\frac{4l_c^2 I^2(\omega) d_{eff}^2}{\pi^2 n^2(\omega)\, n(2\omega)}\right] \sin^2\left(\frac{\pi l_s}{2l_c}\right) \quad (5)$$

In Equation 5, l_s is the thickness of the BBO bulk crystal and $n(\omega)$ and $n(2\omega)$ are the refractive indices at frequencies ω and 2ω, respectively. l_c is the coherence length of the BBO crystal, which is determined by $l_c = \frac{\lambda}{[4(n(\omega)-n(2\omega))]}$, with a typical value of ≈15 μm.[23]

Using Equation 5 and the known efficiency of a 4 mm-thickness BBO bulk crystal (usually ≈1–10%),[43,44] the calculated efficiency of a 114 μm-thickness BBO crystal (the same value as the MNW length) is ≈0.46–4.6%. Therefore, the effective SHG efficiency of BBO single-crystal MNWs is much higher than that of a bulk crystal, which can be explained by the much-tighter confinement of the propagation light in an MNW than in a bulk crystal. Since the morphology of the BBO material has a great influence on the second-harmonic generation efficiency,[27] the SHG conversion efficiency can be further increased by improving the surface quality of the BBO MNWs.

In addition, since the diameter of the MNW is close to the wavelength of the pump light, a certain fractional power of the light may spread out of the solid core of the MNW,[45] which may decrease the SHG conversion efficiency due to the reduced strength of the light-MNW interaction. To investigate the dependence of the SHG conversion efficiency (from a 1064 nm pump to 532 nm signal light) on the MNW diameter, we measured the SHG emission from the ends of 9 MNWs with different diameters (see Supporting Information, Figure S4), and obtained the diameter-dependent SHG efficiency (Figure 4b). It shows that, when the diameter of the MNW increases from 0.79 to 2.2 μm, the SHG efficiency increases monotonously from 2.7% to 8.4%. To explain this dependence, we numerically calculated the Poynting vector of the lowest-order guiding mode on the cross-section plane of the MNW using a Comsol Multiphysics finite-element method (Figure 4c), in which the refractive indices of the MNW and the substrate at 1064 nm wavelength were assumed to be 1.66 (for BBO) and 1.37 (for MgF_2) respectively, and the MNW diameter was measured by the side length (L) of the triangle cross-section. It is clearly shown that the optical confinement of the MNW (i.e., the fractional power inside the triangle cross-section of the MNW) increases monotonously with increasing L. When L = 0.7 μm, the optical confinement of the MNW is very weak, with very low fractional power inside the nonlinear triangle core, indicating low SHG efficiency; when L increases to 0.8 μm, the guiding mode is well confined around the triangle core, but a considerable fractional power is propagated outside the core; when L increases to 2.2 μm, almost all of the power is confined inside the nonlinear core, resulting in a high SHG efficiency.

5. Conclusions

In summary, we have reported the synthesis of free-standing β-BBO MNWs by an organic-free hydrothermal method assisted with post-annealing. The MNWs showed optical-waveguiding capability within the visible and near-IR spectral range. By launching 1064 nm-wavelength picosecond pulses into a single MNW and guiding them through, an evident SHG signal was observed, with a SHG conversion efficiency of about 8.4% in a 2.2 μm-diameter, 114 μm-length BBO MNW. With an MNW diameter close to the wavelength of the pump light, we found that the SHG conversion efficiency increases with the diameter of the BBO MNW. Our results show that, waveguiding β-BBO MNWs are promising 1D building blocks for micro-/nanoscale nonlinear photonic devices.

6. Experimental Section

Preparation of BBO MNWs: BBO MNWs were synthesized by an organic-free hydrothermal method assisted with a post-annealing procedure. To start with, 0.01 mol of $BaCl_2{\cdot}6H_2O$, 0.02 mol of NaOH, and 0.02 mol of H_3BO_3 were dissolved in 15 mL deionized water to form clear solutions. $BaCl_2$ and NaOH solution were mixed and stirred thoroughly to form the $Ba(OH)_2$ emulsion under ultrasound irradiation. Then, H_3BO_3 solution was dipped into the $Ba(OH)_2$ emulsion slowly. After continuous stirring for 30 min, the white slurry was transferred into a stainless-steel autoclave with polytetrafluorethylene (PTFE) (Teflon) lining (volume 55 mL) and heated at temperature of 150–200 °C for 5 days in a preheated oven. A white flocculent precipitate was deposited at the bottom of the autoclave when the reaction finished. After being filtered and washed with deionized water and alcohol several times, we got MNWs in the γ-BaB_2O_4 form. To transform the γ-BaB_2O_4 MNWs to β-BaB_2O_4 MNWs, we annealed the γ-BaB_2O_4 MNWs in a horizontal quartz tube furnace (diameter: 55 mm, length: 1200 mm). Briefly, the as-synthesized γ-BaB_2O_4 MNWs were dipped onto a sapphire substrate after being dispersed with alcohol; then the sapphire substrate was inserted into the center of the tube furnace and heated to 700 °C for 1 h with 100 sccm (standard cubic centimeter) continuous flow of an O_2 atmosphere. After cooling, the as-prepared samples were characterized by an SEM and a TEM equipped with an energy dispersive spectrometer (EDS) detector.

Light Sources: The monochromatic light sources (532 and 671 nm wavelength) used in the optical measurement were continuous-wave lasers. The 1064 nm, picosecond pulses (10 kHz repetition rate, 10 ps pulse width) used for SHG were from a 1064 nm-wavelength YVO_4 picosecond laser.

Measurement of the Intensities from the BBO MNWs: The angle and position of the fiber taper were carefully adjusted so that the coupling was optimized with maximum output observed from the distal end of the BBO MNW. To keep the coupling efficiency constant, the fiber taper was horizontally moved along the axial direction of the BBO MNW without changing the coupling angle between the fiber taper and the MNW. The output images of the other end of BBO MNW with different propagation distances were recorded using a calibrated CCD camera (DXM1200F, Nikon) without saturation. We selected a 60 × 60 pixel area of the captured image with the output spot in the center, and transformed the output image from an RGB image into grayscale information using Adobe Photoshop, and then obtained the normalized output intensity by summing up the gray values; thus, the corresponding intensities of the different propagation distances could be obtained.

Supporting Information

Supporting Information is available from the Wiley Online Library or from the author.

Acknowledgements

This work was supported by the National Natural Science Foundation of China (Grant No. 61036012), the Natural Science Foundation of Zhejiang Province, China (Grant No. Y6110391), and Fundamental Research Funds for the Central Universities. The authors thank Prof. Mo Li, Mr. Tanwei Li, Mr. Zesong Zhang, Dr. Shanshan Wang, Dr. Xining Zhang and Dr. Yaoguang Ma for help discussions.

Received: July 6, 2012
Revised: September 10, 2012
Published online: October 11, 2012

[1] J. T. Hu, T. W. Odom, C. M. Lieber, *Acc. Chem. Res.* **1999**, *32*, 435.
[2] Y. N. Xia, P. D. Yang, Y. G. Sun, Y. Y. Wu, B. Mayer, B. Gates, Y. D. Yin, F. Kim, H. Q. Yan, *Adv. Mater.* **2003**, *15*, 353.
[3] T. Voss, G. T. Svacha, E. Mazur, S. Müller, C. Ronning, D. Konjhodzic, F. Marlow, *Nano Lett.* **2007**, *7*, 3675.
[4] Y. Nakayama, P. J. Pauzauskie, A. Radenovic, R. M. Onorato, R. J. Saykally, J. Liphardt, P. D. Yang, *Nature* **2007**, *447*, 1098.
[5] D. I. Yeom, E. C. Maegi, M. R. E. Lamont, M. A. F. Roelens, L. B. Fu, B. J. Eggleton, *Opt. Lett.* **2008**, *33*, 660.
[6] B. Yan, L. Liao, Y. M. You, X. J. Xu, Z. Zheng, Z. X. Shen, J. Ma, L. M. Tong, T. Yu, *Adv. Mater.* **2009**, *21*, 2436.
[7] L. X. Jia, M. M. Geng, L. Zhang, L. Yang, P. Chen, T. Wang, Y. L. Liu, *Opt. Commun.* **2009**, *282*, 1659.
[8] B. A. Daniel, G. P. Agrawal, *J. Opt. Soc. Am. B* **2010**, *27*, 956.
[9] H. Hu, H. Ji, M. Galili, M. H. Pu, C. Peucheret, H. Christian, H. Mulvad, K. Yvind, J. M. Hvam, P. Jeppesen, L. K. Oxenløwe, *Opt. Express* **2011**, *19*, 19886.
[10] F. X. Gu, H. K. Yu, W. Fang, L. M. Tong, *Opt. Express* **2012**, *20*, 8667.
[11] L. W. Tutt, T. F. Boggess, *Prog. Quantum Electron.* **1993**, *17*, 299.
[12] K. Brunner, G. Abstreiter, G. Böhm, G. Tränkle, G. Weimann, *Phys. Rev. Lett.* **1994**, *73*, 1138.
[13] T. K. Liang, H. K. Tsang, *Appl. Phys. Lett.* **2004**, *84*, 2745.
[14] H. S. Rong, A. S. Liu, R. Nicolaescu, M. Paniccia, O. Cohen, D. Hak, *Appl. Phys. Lett.* **2004**, *85*, 2196.
[15] H. S. Rong, R. Jones, A. S. Liu, O. Cohen, D. Hak, A. Fang, M. Paniccia, *Nature* **2005**, *433*, 725.
[16] A. Magrez, E. Vasco, J. W. Seo, C. Dieker, N. Setter, L. Forro, *J. Phys. Chem. B* **2006**, *110*, 58.
[17] J. Y. Huang, Z. Chen, Z. S. Zhang, C. Y. Zhu, H. P. He, Z. Z. Ye, G. Y. Qu, L. M. Tong, *Appl. Phys. Lett.* **2011**, *98*, 093102.
[18] F. Dutto, C. Raillon, K. Schenk, A. Radenovic, *Nano Lett.* **2011**, *11*, 2517.
[19] D. N. Nikogosyan, *Appl. Phys. A* **1991**, *52*, 359.
[20] D. A. Keszler, *Curr. Opin. Solid State Mater. Sci.* **1996**, *1*, 204.
[21] D. A. Keszler, *Curr. Opin. Solid State Mater. Sci.* **1999**, *4*, 155.
[22] T. Sasaki, Y. Mori, M. Yoshimura, Y. K. Yap, T. Kamimura, *Mater. Sci. Eng. R* **2000**, *30*, 1.
[23] C. T. Chen, B. C. Wu, A. D. Jiang, G. M. You, *Sci. Sin., Ser. B* **1985**, *28*, 235.
[24] D. Eimerl, L. Davis, S. Velsko, E. K. Graham, A. Zalkin, *J. Appl. Phys.* **1987**, *62*, 1968.
[25] P. Becker, *Adv. Mater.* **1998**, *10*, 979.
[26] C. Lu, S. S. Dimov, R. H. Lipson, *Chem. Mater.* **2007**, *19*, 5018.
[27] Q. R. Zhao, X. Zhu, X. Bai, H. H. Fan, Y. Xie, *Eur. J. Inorg. Chem.* **2007**, *13*, 1829.
[28] R. Li, X. Y. Tao, X. D. Li, *J. Mater. Chem.* **2009**, *19*, 983.
[29] J. Zhang, S. J. Liang, G. P. He, *Chem. Lett.* **2009**, *38*, 500.
[30] W. J. Li, E. W. Shi, W. Z. Zhong, Z. W. Yin, *J. Cryst. Growth* **1999**, *203*, 186.
[31] S. H. Feng, R. R. Xu, *Acc. Chem. Res.* **2001**, *34*, 239.
[32] C. N. R. Rao, F. L. Deepak, G. Gundiah, A. Govindaraj, *Prog. Solid. State. Chem.* **2003**, *31*, 5.
[33] B. L. Cushing, V. L. Kolesnichenko, C. J. O'Connor, *Chem. Rev.* **2004**, *104*, 3893.
[34] X. Wang, J. Zhuang, Q. Peng, Y. D. Li, *Nature* **2005**, *437*, 121.
[35] X. Wang, Y. D. Li, *Inorg. Chem.* **2006**, *45*, 7522.
[36] O. Yamaguchi, K. Tominaga, K. Shimizu, *Ceram. Int.* **1980**, *6*, 103.
[37] L. M. Tong, R. R. Gattass, J. B. Ashcom, S. L. He, J. Y. Lou, M. Y. Shen, I. Maxwell, E. Mazur, *Nature* **2003**, *426*, 816.

[38] L. M. Tong, J. Y. Lou, R. R. Gattass, S. L. He, X. W. Chen, L. Liu, E. Mazur, *Nano. Lett.* **2005**, *5*, 259.
[39] A. L. Pyayt, B. Wiley, Y. N. Xia, A. T. Chen, L. Dalton, *Nat. Nanotechnol.* **2008**, *3*, 660.
[40] Y. G. Ma, X. Y. Li, H. K. Yu, L. M. Tong, Y. Gu, Q. H. Gong, *Opt. Lett.* **2010**, *35*, 1160.
[41] Y. R. Shen, *The Principles of Nonlinear Optics*, Wiley, New York **1984**, Ch. 7.
[42] H. A. Lu, L. A. Wills, B. W. Wessels, W. P. Lin, T. G. Zhang, G. K. Wong, D. A. Neumayer, T. J. Marks, *Appl. Phys. Lett.* **1993**, *62*, 1314.
[43] T. Yogo, K. Kikuta, K. Niwa, M. Ichida, A. Nakamura, S. Hirano, *Proc. SPIE* **1994**, *2288*, 484.
[44] T. Yogo, K. Niwa, K. Kikuta, M. Ichida, A. Nakamurab, S. Hirano, *J. Mater. Chem.* **1997**, *7*, 929.
[45] L. M. Tong, J. Y. Lou, E. Mazur, *Opt. Express* **2004**, *12*, 1025.